Sorption Thermodynamics of CO_2, CH_4, and Their Mixtures in the ITQ-1 Zeolite as Revealed by Molecular Simulations

Jean-Marc Leyssale, George K. Papadopoulos, and Doros N. Theodorou*

School of Chemical Engineering, National Technical University of Athens, 9 Heroon Polytechniou Street, Zografou Campus, 15780 Athens, Greece

Received: August 1, 2006

The thermodynamic properties and siting of carbon dioxide and methane sorbed in the siliceous form of zeolite MCM-22, ITQ-1, were studied by means of grand canonical Monte Carlo simulation. ITQ-1 comprises two independent pore systems of different geometry. It was found to be CO_2-selective toward CO_2/CH_4 gas mixtures, its equilibrium selectivity being distinctly higher in its sinusoidal channel pore system than in the large cavity system over a wide range of pressures starting from the Henry law regime, at the three temperatures considered. A maximum in selectivity is observed at low temperature, high pressure, and methane-rich gas-phase composition.

1. Introduction

Natural gas is a mixture of hydrocarbons (mainly CH_4), water, and acid gases, such as CO_2 and H_2S. Since water and acid gases decrease the energy content of the gas and can be responsible for the corrosion of pipelines, their separation from the gas mixture is of tremendous industrial interest.[1] Of particular interest is the separation of CO_2 and CH_4, as the storage of these two greenhouse effect gases is also a fundamental environmental issue.[2] Separation through micro- or nanoporous membranes has emerged in recent years as a highly valuable and economical tool as compared with other techniques, such as cryogenics or high-pressure pumping.[3] Membrane materials can be distinguished into amorphous, such as activated carbons, and crystalline, such as zeolites. Separation of two species by using a porous crystalline material can result from different microscopic mechanisms that can be related to equilibrium thermodynamics or to kinetics. For two species presenting very different kinetic diameters (the kinetic diameter of a molecule being the minimum diameter of a cylindrical pore in which the molecule can fit) a zeolite with cylindrical straight channel pores of diameter intermediate between the diameters of the two species will be highly selective. Due to their low and similar kinetic diameters (0.33 nm for CO_2 and 0.38 nm for CH_4) only a few small pore zeolites are possible candidates for such a separation process of these two molecules. Up to now, CO_2/CH_4 separation has been reported in two types of small pore zeolites: SAPO-34[4−8] (0.38 nm pore diameter) and DDR[9] (0.36×0.44 nm^2). These studies showed interesting selectivities for both membranes. Adsorption of water molecules in SAPO-34, a highly hydrophilic silicoaluminophosphate, has, however, been shown to block the zeolite pores.[7] Adsorption and permeation of CO_2 and/or CH_4 have also been investigated experimentally in large pore size FAU-X[10] and FAU-Y[11] and medium pore size MFI[12−19] zeolites. In these cases, the pore size diameters are larger than all kinetic diameters of the sorbates and selectivity results from a combination of competitive adsorption, an equilibrium thermodynamic property, and differences in transport properties of the sorbates inside the material, a kinetic property. MCM-22 (ISA code MWW) is a recently synthesized low Al/Si ratio aluminosilicate zeolite possessing an unusual framework structure made of two independent large pore systems, offering a variety of possible sorption sites.[20] One of the pore systems is composed of two-dimensional sinusoidal ten-member ring (10-MR) channels (SC) with a pore diameter of 0.4−0.55 nm and the other one of large 12-MR cavities (LC) of dimensions 1.7×0.8 nm^2, connected by 10-MR windows. In view of its large pore systems, MCM-22 has been mainly studied in the context of large hydrocarbon adsorption for catalytic purposes.[21,22] The high void space density of the MWW topology, together with its unique crystal structure, make it also very interesting in the context of small gas adsorption and separation. The recently proposed ITQ-1 zeolite,[23] the fully siliceous variant of MCM-22, is of particular interest for natural gas separation, since this material is hydrophobic.

Molecular simulation techniques are now widely used to investigate sorption and transport properties of sorbates in zeolites.[24] The aim of the work reported in this article is to investigate by Grand Canonical Monte Carlo (GCMC) simulations the sorption properties of the ITQ-1 zeolite with respect to CO_2/CH_4 mixtures. Particular attention is paid to understanding the role of the crystalline structure, the external conditions (temperature, gas pressure, and composition), and the intermolecular interactions on the sorbed amounts and structure of the mixed sorbed fluid phase inside the material. The transport properties of the same gases in this zeolite will be the object of a forthcoming publication.

The article is organized as follows. In section 2 we describe the structural features of the zeolite, the interatomic potentials we used to model ITQ-1, CO_2, CH_4, and their mutual interactions, and the basic features of the simulation methodology. Single-component adsorption results are then discussed in section 3 and mixture adsorption in section 4.

2. Simulation Details

We constructed a model for the ITQ-1 zeolite framework according to the crystallographic data of Camblor et al.[23] For

* To whom correspondence should be addressed. Phone: +30-210-772-3157. Fax: +320-210-772-3112. E-mail: doros@central.ntua.gr.

10.1021/jp064918+ CCC: $33.50
Published on Web 10/19/2006

TABLE 1: Lennard-Jones Interaction Parameters and Partial Charges for the Sorbate and Sorbent Models Used in This Work

name	site	ϵ (kcal/mol)	σ (Å)	partial charge (e)
ITQ-1	Si	none	none	+2
	O	0.177932	2.806	−1
EPM2	C	0.055858	2.757	+0.6512
	O	0.159870	3.033	−0.3256
GWMWQ	CH_4	0.293799	3.73	
DCVKMS	CH_4	0.314749	3.72	

convenience with periodic boundary conditions we used a double unit cell instead of the original hexagonal one. This new unit cell has an orthorhombic shape with axes $a = 2\cos(60°)a'$; $b = a'$; $c = c'$, where a' and c' are the original hexagonal unit cell axes. This created a base-centered orthorhombic unit cell with lattice points located at the centers of large cavities of the zeolite. This unit cell is composed of 144 silicon and 288 oxygen atoms. The whole zeolite is treated as a rigid body in all calculations. Lennard-Jones interaction sites are assigned to oxygen atoms and partial charges of +2e and −1e are assigned to silicon and oxygen atoms, respectively.[25]

Carbon dioxide is described, as in previous work on CO_2 in silicalite,[25] by the EPM2 model of Harris and Yung.[26] This model is composed of Lennard-Jones centers and partial charges on carbon and oxygen atoms. The CO_2 molecule is treated as a rigid linear body with a C−O bond length of 1.149 Å. Methane molecules are described by two united atom interaction potentials that have been invoked in the past to model CH_4−silicalite systems: the potential due to Goodbody et al.[27] (referred to here as GWMWQ), and the one due to Dubbeldam et al.[28] (noted as DCVKMS). These two models represent CH_4 as a single Lennard-Jones interaction site. All interaction parameters used in our calculations are given in Table 1. Cross Lennard-Jones interaction terms between the zeolite oxygen atoms and the DCVKMS methane sites have been assigned specific zeolite/methane cross parameters of $\epsilon = 0.228367$ kcal/mol and $\sigma = 3.47$ Å. All other cross terms are obtained through the Lorentz−Berthelot combining rules. On one hand the use of the GWMWQ potential is attractive, since all compounds (sorbates and sorbent) possess their own Lennard-Jones parameters and cross terms are obtained in a consistent way through combining rules. On the other hand, the recently proposed DCVKMS potential, fitted to reproduce sorption isotherms in MFI zeolites, is thought to be more accurate and transferable than the GWMWQ one.

Comparison of results obtained with these two potentials will highlight the dependence of the presented results on the sorbate model. Note that all potential models used in this work have previously shown a good ability to reproduce sorption experiments in silicalite. It is thus reasonable to use them for computer experiments of adsorption in ITQ-1, another fully siliceous zeolite. Adopting a rigid zeolite model allowed us to use the pretabulation/interpolation scheme for sorbate/sorbent interactions introduced by June et al.[29] All van der Waals interactions are computed within a cutoff distance of 13 Å. This cutoff is also applied to CO_2/CO_2 Coulombic interactions, whereas long-range CO_2/sorbent electrostatics is computed explicitly and pretabulated by using the Ewald summation technique. We checked the effect of the truncation of CO_2/CO_2 electrostatic interactions by computing the sorption isotherm at $T = 300$ K using full Ewald summation without any cutoff. The resulting isotherms were absolutely identical with the one presented in Figure 1a in the absence of long-range guest/guest electrostatics. Note that, since the guest/host interactions are tabulated, they have to be computed only once for all potential map grid points and for all sorbate atom/sorbent pairs. This makes the use of Ewald summation very inexpensive in that context.

TABLE 2: Henry Constant K_H (molecules/u.c./atm) and Isosteric Heat of Adsorption q_{st} (kcal/mol) at Zero Loading ($P \rightarrow 0$) of Carbon Dioxide and Methane (DCVKMS and GWMWQ models)

		CO_2			CH_4 (DCVKMS)			CH_4 (GWMWQ)		
T (K)		total	LC	SC	total	LC	SC	total	LC	SC
300	K_H	19.6	4.2	15.4	9.1	4.1	5.0	6.2	3.2	3.0
	q_{st}	5.888	4.658	6.218	4.787	4.438	5.077	4.287	4.138	4.457
275	K_H	49.1	8.7	40.4	18.9	8.0	10.9	12.0	6.1	5.9
	q_{st}	5.988	4.719	6.258	4.807	4.468	5.057	4.297	4.167	4.427
250	K_H	148.7	20.7	128.0	45.7	18.2	27.5	26.4	13.1	13.3
	q_{st}	6.099	4.799	6.309	4.827	4.518	5.037	4.307	4.217	4.407

Sorption isotherms of pure compounds and mixtures are computed through Grand Canonical Monte Carlo (GCMC) simulations as proposed by Adams.[30,31] Monte Carlo moves include insertions, deletions, translations, rotations (CO_2 only), and identity exchanges (binary mixtures only), attempted with equal probabilities. All simulations are performed in a box of $2 \times 3 \times 2$ orthorhombic unit cells. Simulations of pure compounds comprise 25 blocks of 10^6 MC steps to thermalize the systems and 100 blocks to compute averages. For the mixtures we use respectively 25 and 100 blocks of 4×10^5 steps for the thermalization and production runs. Block averaging is used to compute error bars (one standard deviation). The last configuration obtained at one pressure is used as the initial configuration for thermalization at a higher pressure.

3. Pure Sorbate Results

We first discuss results concerning the sorption of pure sorbates in the limit of zero pressure. Henry constants and isosteric heats of adsorption are presented in Table 2. Total quantities predicted from the simulation have been partitioned into contributions coming from the large cavities (LC) and the sinusoidal channels (SC) of the zeolite. It is worth mentioning the excellent agreement between isosteric heat values (q_{st}) in the limit of zero coverage extracted from our MC simulations and reported in Table 2 and Figure 4, and the ones calculated from the temperature dependence of K_H by the thermodynamic relation

$$q_{st} = R\frac{\partial \ln K_H}{\partial(1/T)}$$

As expected, the Henry constant increases as temperature decreases. Both Henry constants and heats of adsorption indicate stronger adsorption for carbon dioxide than for methane, due to the ability of CO_2 to develop electrostatic interactions with the sorbent framework. We can also see that Henry constants are higher, slightly higher, and similar in the narrow SC than in the large LC pores for carbon dioxide, DCVKMS methane, and GWMWQ methane, respectively. This result sounds surprising if we consider that the accessible volume to the sorbates in the LC is approximately 2.8 times the one in the SC and so we could expect higher Henry constants in LC than in SC. This ratio of 2.8 has been determined through a 1 μs NVE molecular dynamics simulation of 144 DCVKMS methane molecules at $T = 800$ K in a 96 unit cell simulation box. We found accessible volumes of 13.25% and 4.7% of the full zeolite volume for the LC and SC pore systems, respectively. These accessible volumes are outlined with gray surfaces in Figure 1. However, as can be seen in Figure 1, the SC pore system is quite uniform in size and its size is similar to the

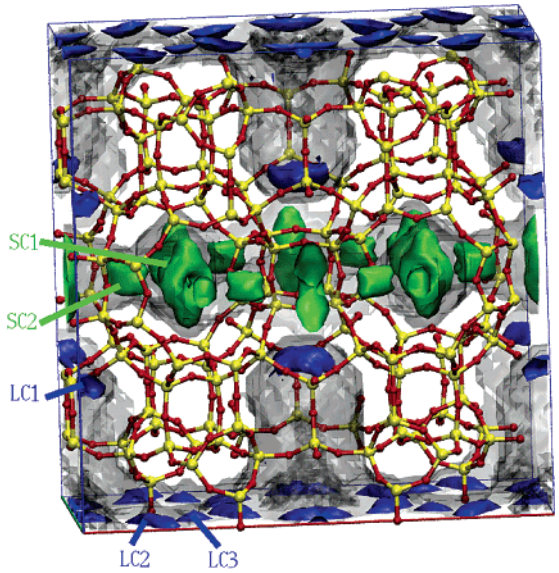

Figure 1. Isodensity surfaces showing the highest probability sorption sites of carbon dioxide obtained in a GCMC simulation in the Henry regime at 250 K. Sorption sites in SC are shown in green and those in LC in blue. The gray surfaces outline the accessible space in both pore systems.

sizes of sorbate molecules. SC thus presents a very favorable environment for both sorbates. On the contrary, LC presents very large side pockets communicating via large 12-member-ring (MR) openings in the *z* direction and narrow channels in the *xy* plane. Consequently, only a few locations inside the LC are able to form strong interactions with the sorbates. This point is highlighted in Figure 1, where high-density probability isosurfaces (in other words, highly favorable sorption sites) are shown for these two pore systems. (Displayed isosurfaces refer to CO_2 at 250 K in the Henry law regime; isosurfaces in SC correspond to a higher density level than the ones in LC.) We can see in this figure that highly favorable sorption sites exist all along the SC (sites SC1 and SC2), whereas they are localized only at the top of the supercages (LC1), along the 12 MR openings (LC2) and in the intercavity spaces (LC3) in LC. Values of the heat of adsorption, higher for both sorbates in SC than in LC, confirm this picture. Finally, we point out that the DCVKMS model of methane gives significantly higher Henry constants and heats of adsorption than the GWMWQ one. In LC the values obtained with this model are quite close to the ones obtained for carbon dioxide.

Figure 2 shows sorption isotherms for CO_2 at $T = 300$ (a), 275 (b), and 250 K (c) and for the DCVKMS (filled symbols) and GWMWQ (open symbols) models of methane at $T = 300$ (d), 275 (e) and 250 K (f). The full zeolite loadings are shown with circles and the corresponding LC and SC components with squares and triangles, respectively.

All error bars (not shown) are of the same order or smaller than the symbol sizes. First we can see that for all temperatures and pressures the zeolite sorbs more carbon dioxide than methane. We can also see that the two methane models give similar isotherms until around 10 atm and then go to slightly different plateau values, the GWMWQ model presenting higher plateau values than the DCVKMS one. Comparison between our simulated isotherms for CO_2 with preliminary experimental results on CO_2 in MCM-22[32] shows that our simulations underestimate the sorbed amounts of gas at low pressure and overestimate them at high pressure. The low-pressure underestimation can result from the presence of aluminum (creating stronger electric fields) in the MCM-22 framework and the high-

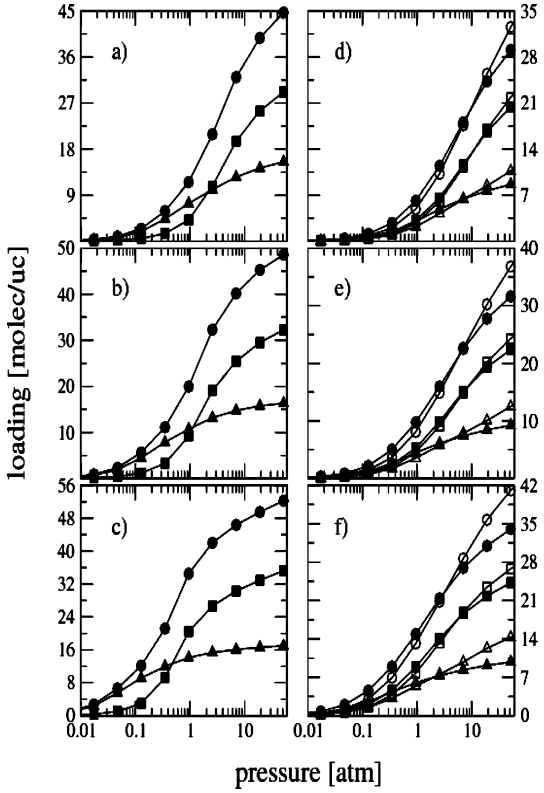

Figure 2. Sorption isotherms of carbon dioxide at 300 (a), 275 (b), and 250 K (c) and of methane (filled symbols: DCVKMS; open symbols: GWMWQ) at 300 (d), 275 (e), and 250 K (f). Circles: total loading; squares: LC loading; triangles: SC loading.

pressure overestimation from the presence of extraframework counterions or defects in the real crystals. We now discuss in more detail the contributions of the two pore systems to the sorption isotherms, which are quite different for CO_2 and CH_4. At low pressure CO_2 is mainly sorbed in SC, sorption in LC taking place at a slightly higher pressure. For instance, we see that at $T = 250$ K and $P = 0.1$ atm, SC is half-filled by CO_2 whereas LC is only 5% filled. At $P = 1$ atm, SC is almost fully filled and LC only half-filled. In the case of methane, LC and SC loadings are of the same order until a pressure of 1 atm and then go toward their respective plateau values as pressure increases. This picture is confirmed in Figure 3. This figure shows the ratio of the molar fraction of molecules in SC and LC: X_{SC}/X_{LC}, as well as the scaled ratio taking into account the accessible volumes of the two pore systems: $X_{SC}V_{LC}/(X_{LC}V_{SC})$. We can see that for both sorbates the unscaled ratios at low pressure correspond to the ratios of the Henry constants in the two pore systems. The values of this ratio for CO_2 at low pressure, ranging from 3.6 at $T = 300$ K to 6 at $T = 250$ K, are much higher than those for methane (from 1.2 to 1.5 for the DCVKMS model and from 0.9 to 1 for the GWMWQ). These high values confirm that at low pressures CO_2 is almost exclusively sorbed in SC. At higher pressures, when the SC is almost fully occupied, sorption starts to take place in LC and the ratios decrease. In the case of methane, the low pressure values of the ratio between 0.9 and 1.5, depending on model and temperature, indicate that both pore systems are filled more or less equally with similar amounts of gas. When pressure is increased, as for CO_2, the smaller SC are fully occupied and the ratios decline as CH_4 continues to be sorbed in LC. Note that at high pressures the scaled ratio values approach one for all sorbates, as expected for a fully occupied zeolite.

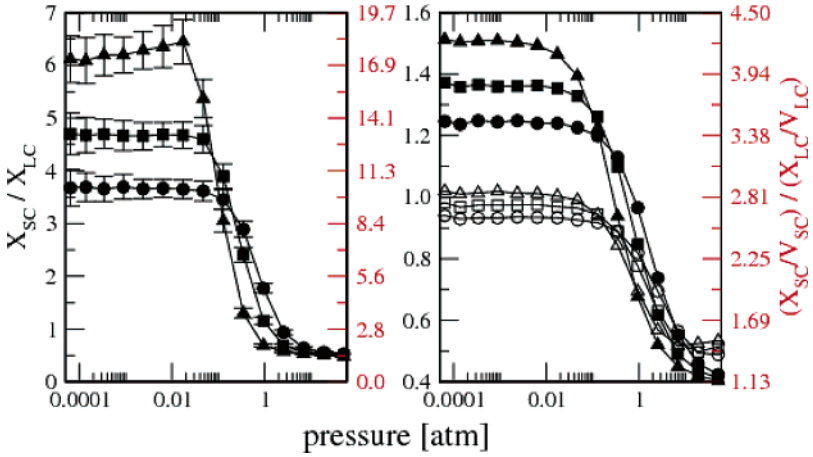

Figure 3. SC over LC loading ratio (left scale) and the same ratio scaled by the volume of each pore system (right scale) for carbon dioxide (left), DCVKMS (right, filled symbols), and GWMWQ (right, open symbols) methane. Circles: $T = 300$ K; squares: $T = 275$ K; triangles: $T = 250$ K.

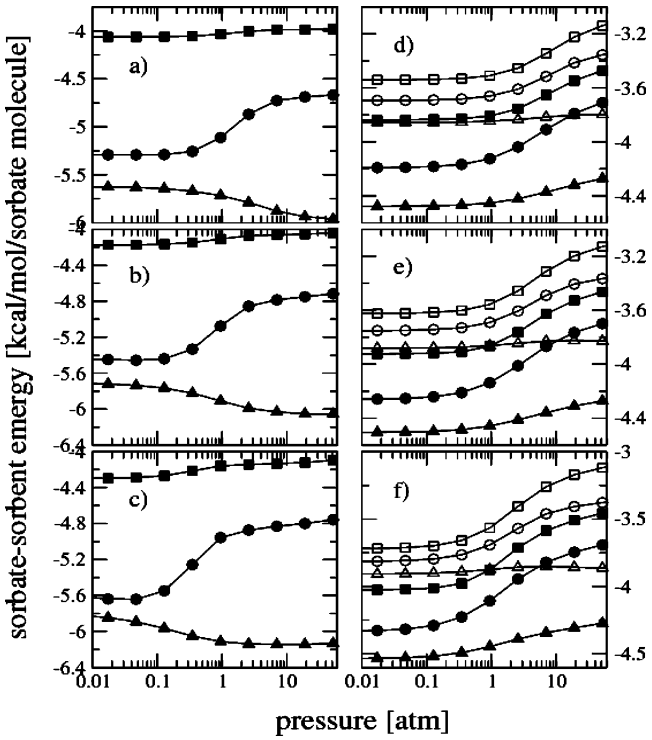

Figure 4. Evolution with pressure of the sorbate/sorbent interaction energy for carbon dioxide at 300 (a), 275 (b), and 250 K (c) and for methane (filled symbols: DCVKMS; open symbols: GWMWQ) at 300 (d), 275 (e), and 250 K (f). Circles: total zeolite; squares: LC; triangles: SC.

The evolution with pressure of the sorbate/sorbent interaction energy per sorbate molecule is shown in Figure 4 for CO_2 at $T = 300$ (a), 275 (b), and 250 K (c) and for methane at $T = 300$ (d), 275 (e), and 250 K (f). We first see that, as noted for the heat of adsorption, sorbate/sorbent interactions are always stronger in SC than in LC. Moreover, their evolution with pressure presents quite different behavior in LC and in SC. In the case of CO_2 we see that for pressures out of the Henry regime, the CO_2/sorbent energy in LC increases slightly with pressure. This stems from the fact that out of the Henry regime molecules start occupying less favorable sites in LC. On the contrary, the CO_2/sorbent energy decreases with pressure in SC, showing an ordering transition in this pore system as pressure increases. The resulting total sorbate/sorbent interaction energies, which are constant at low pressure, show well-pronounced increases before reaching a higher plateau value at high pressures. This increase corresponds to the point at which the SC are fully filled and where the less favorable LC start to be filled. In the case of methane, Figure 4d,e,f confirms first that sorbate/sorbent interaction energies are more attractive for DCVKMS CH_4 than for GWMWQ CH_4 for all pressures and temperatures.

The evolution of sorbate energy with loading in LC is similar between the two models and also to what has been observed in the case of CO_2, displaying an increase due to sorption in less favorable sites. The behavior of the sorbate/sorbent interaction energy in SC is, however, very different for methane than for CO_2: Both models show an increase of the interaction energy with pressure in SC; this increase is more pronounced for the DCVKMS model than for the GWMWQ model. The evolution of the total CH_4/sorbent energy is similar to the one observed for CO_2, for the same reasons.

The average sorbate/sorbate interaction energies per sorbate molecule are shown in Figure 5. The pair energy decreases regularly with pressure for both sorbates. As expected, interactions are stronger for CO_2 than for CH_4 and their strength increases as temperature decreases. We can also see that the two methane models give similar pair energies.

Finally, we show in Figure 6 the evolution of the total sorbate energy per sorbate molecule. The results obtained for the two sorbates are quite different. In the case of CH_4 the total energy increases with pressure at high pressure, whereas it decreases in the case of CO_2. The maxima observed in the case of CO_2 around 1 atm result from a compromise between the increasing sorbate/sorbent energy and the decreasing sorbate/sorbate energy.

Figures 7 and 8 confirm the results presented above. Figure 7 shows contour plots of the sorbate probability density in the *xy* plane for the LC at low ($P = 0.006$ atm), intermediate ($P = 0.95$ atm), and high ($P = 52$ atm) loadings. We can see from Figure 7a that CO_2 exhibits similar probability densities in sites LC1, LC2, and LC3 in the Henry regime. As pressure is increased, we can see in Figure 7b,c that the probability density increases in LC1 and drops in LC2 and LC3. At saturation, carbon dioxide density is high in the LC pockets LC1, intermediate in the intercavity area LC3, and low in the 12 MR area LC2. The case of methane is slightly different. In the Henry regime (Figure 7d,g), methane resides mainly in sites LC1 and LC3, as can be seen in Figure 7c for CO_2 at saturation. When pressure is increased (Figure 7, panels e,f and h,i) the CH_4 density decreases in LC1 and LC3 and increases in LC2,

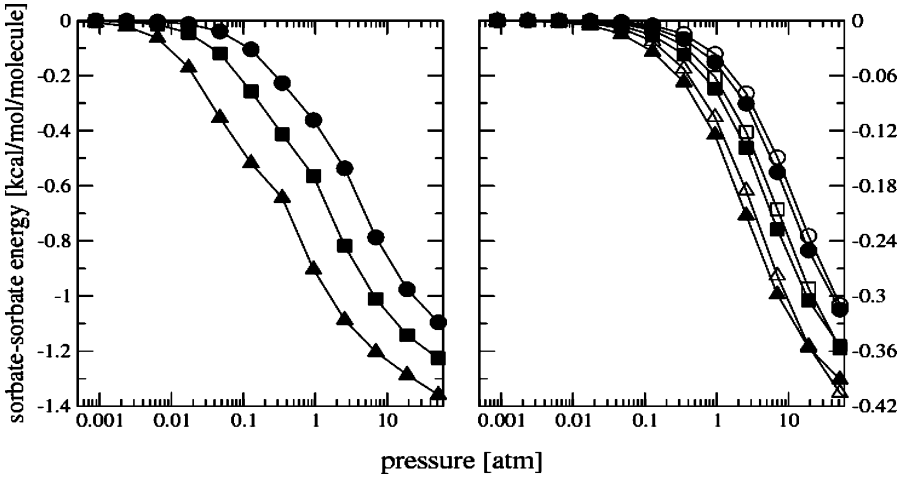

Figure 5. Evolution with pressure of the sorbate/sorbate interaction energy for CO_2 (left), DCVKMS (right, filled symbols), and GWMWQ (right, open symbols) methane. Circles: $T = 300$ K; squares: $T = 275$ K; triangles: $T = 250$ K.

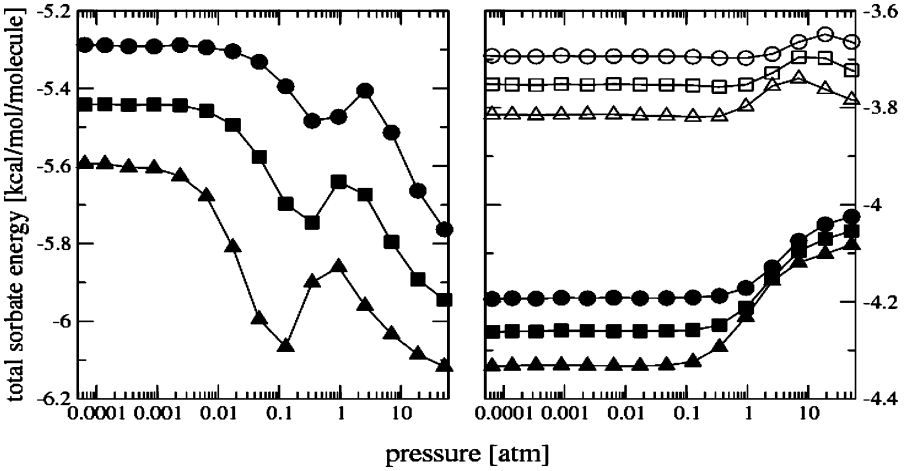

Figure 6. Evolution with pressure of the total sorbate energy for CO_2 (left), DCVKMS (right, filled symbols), and GWMWQ (right, open symbols) methane. Circles: $T = 300$ K; squares: $T = 275$ K; triangles: $T = 250$ K.

resulting in density maps at saturation similar to what is observed for CO_2 at low pressure.

Figure 8 shows plots of the sorbate probability densities in the *xy* plane for the SC at the same state points as in Figure 7. We see in Figure 8a that CO_2 occupies both SC1 and SC2 sites in the Henry regime.

When pressure is increased to around 1 atm (Figure 8b) peaks corresponding to SC1 sites become around 4 times higher than they were in the Henry regime, confirming the ordering transition discussed in connection with Figure 4. No difference is observed between Figure 8b (0.95 atm) and Figure 8c (52 atm), since SC are already almost saturated at 0.95 atm. Panels d and g of Figure 8 show that methane resides mainly in SC1 sites at low pressure. At 0.95 atm (Figure 8e,h) SC2 sites start to be filled and both SC1 and SC2 sites are saturated at 52 atm (Figure 8f,i). We point out that no ordering transition similar to the one observed for carbon dioxide is observed in the case of methane.

4. Mixture Results

The sorption of carbon dioxide/methane mixtures in ITQ-1 is now discussed. Sorption isotherms obtained at $T = 300$, 275, and 250 K for CO_2 mole fraction in the gas phase ranging from 0.1 to 0.9 are shown in Figure 9. The corresponding LC and SC components are shown in Figures 10 and 11, respectively. In each figure, isotherms a, b, and c correspond to CO_2/DCVKMS CH_4 mixtures at respectively 300, 275, and 250 K and isotherms d, e, and f correspond to CO_2/GWMWQ CH_4 mixtures at respectively 300, 275, and 250 K. CO_2 loadings are displayed with filled symbols and methane loadings with open symbols. The CO_2 mole fraction y_{CO_2} (or partial pressure) in the ideal gas mixture evolves from 0.1 (circles) to 0.9 (stars) in steps of 0.1. The first point to note is that CO_2 isotherms obtained with the two methane models are almost identical. Some slight differences can be observed in the methane isotherms obtained with the two models as for pure methane sorption isotherms. These isotherms show a strong selectivity for CO_2 adsorption over CH_4. For instance, looking at the global isotherms (Figure 9) we see that, for all pressures displayed, the sorbed amount of CO_2 is higher than that of CH_4 for $y_{CO_2} \geq 0.2$ at 250 K, $y_{CO_2} \geq 0.2-0.3$ at 275 K, and $y_{CO_2} \geq 0.3$ at 300 K.

If we now look at the LC (Figure 10) and SC (Figure 11) isotherms, we see that LC is weakly CO_2 selective, whereas SC is strongly CO_2 selective. We can see in particular that the sorbed amounts of CO_2 in SC (Figure 11) are higher than those of CH_4 for almost all pressures and compositions at $T = 250$ K. We plot in Figure 12 the loadings of CO_2 obtained for y_{CO_2} ranging from 0.1 to 1 as a function of the partial pressure of CO_2 in the gas phase. Panels a, b, and c of Figure 12 (respectively d, e, and f) correspond to CO_2/DCVKMS CH_4 (respectively CO_2/GWMWQ CH_4) mixtures at $T = 300$, 275,

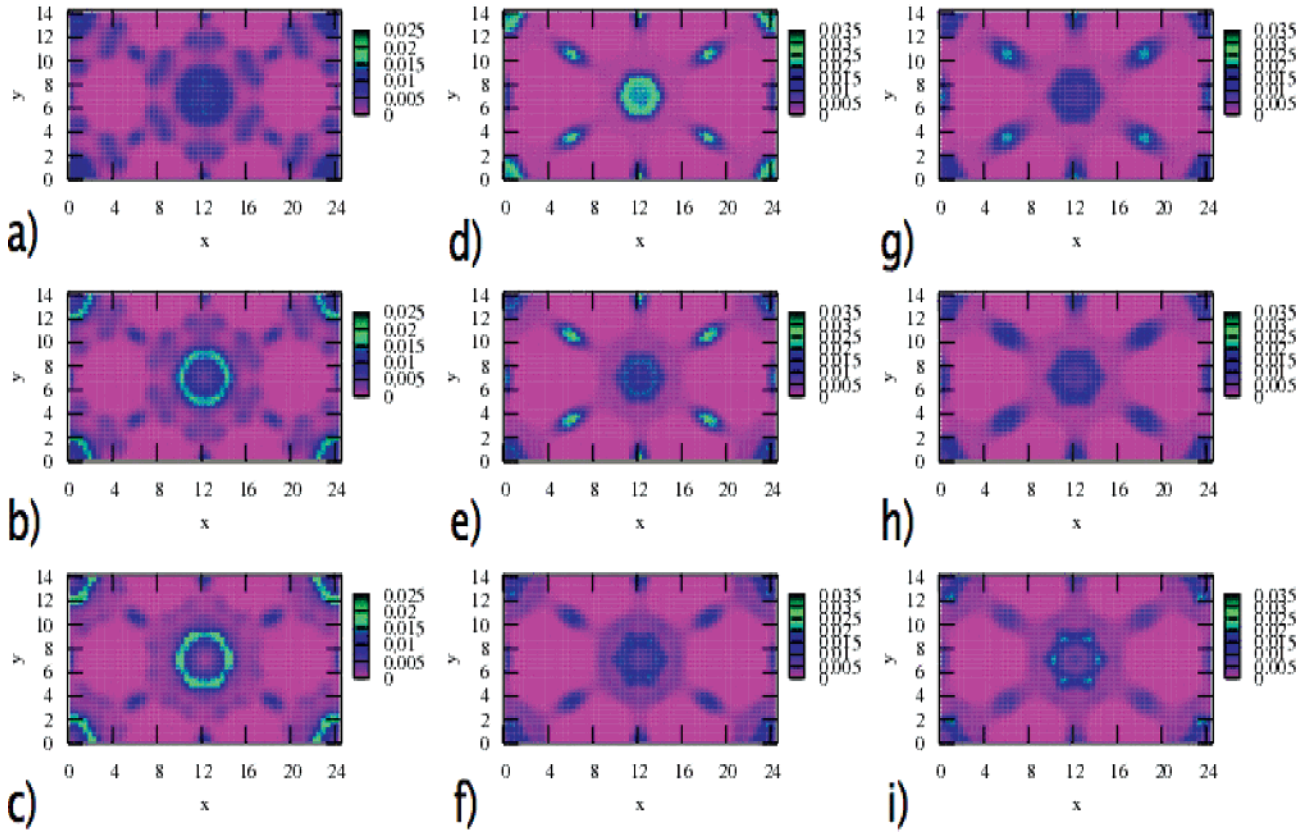

Figure 7. *xy* probability densities for the sorbates in the large cavities at $T = 250$ K. CO_2 at $P = 0.006$ (a), 0.95 (b), and 52 atm (c). (d, e, f) and (g, h, i) are similar to (a, b, c) for DCVKMS and GWMWQ methane, respectively.

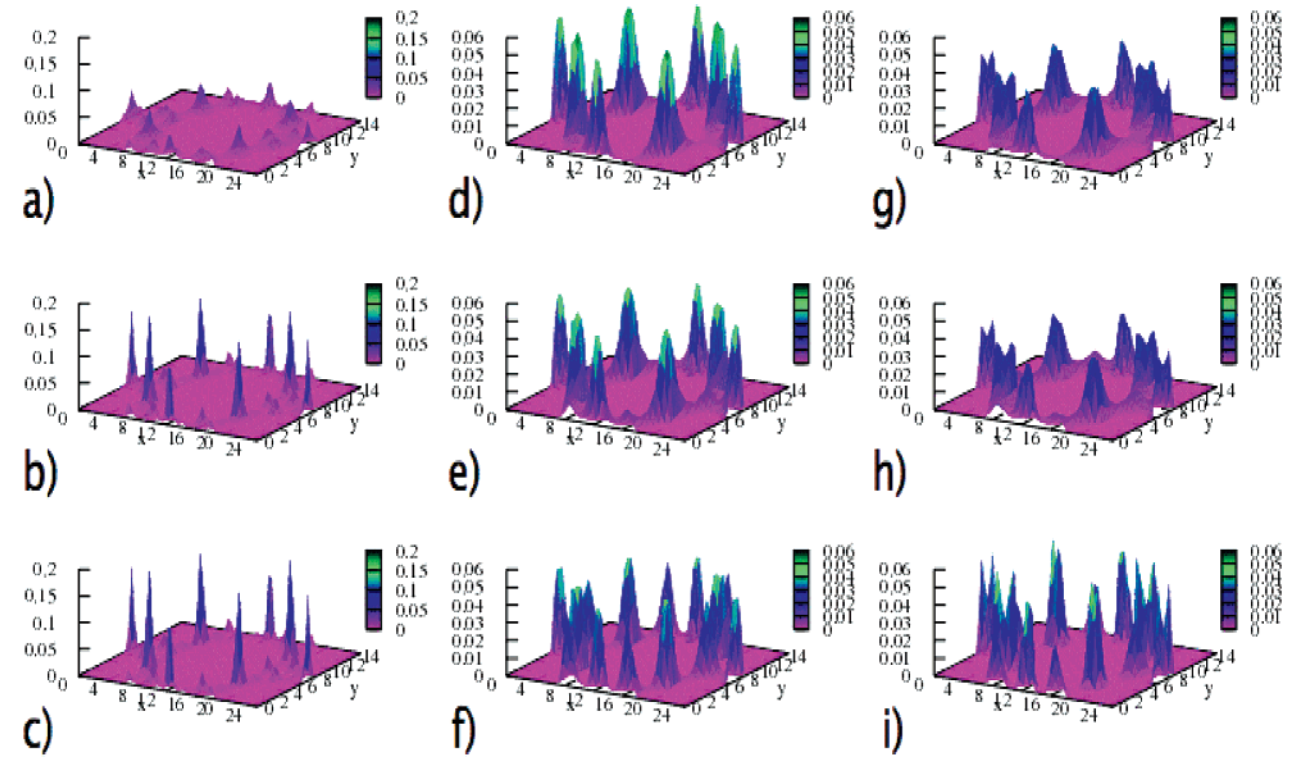

Figure 8. *xy* probability densities for the sorbates in the sinusoidal channels at $T = 250$ K. CO_2 at $P = 0.006$ (a), 0.95 (b), and 52 atm (c). (d, e, f) and (g, h, i) are similar to (a, b, c) for DCVKMS and GWMWQ methane, respectively.

and 250 K. Panels g−*l* and m−r of Figure 12 are the LC and SC components of panels a−f of Figure 12 a to f. These figures show clearly that CO_2 loadings are only little affected by the presence of methane in the gas phase.

This is particularly the case in the sinusoidal channels, for which the presence of methane seems to affect carbon dioxide sorption only at high pressures and methane-rich gas compositions ($y_{CO_2} \leq 2$). Figure 13 is the analogue of Figure 12 for

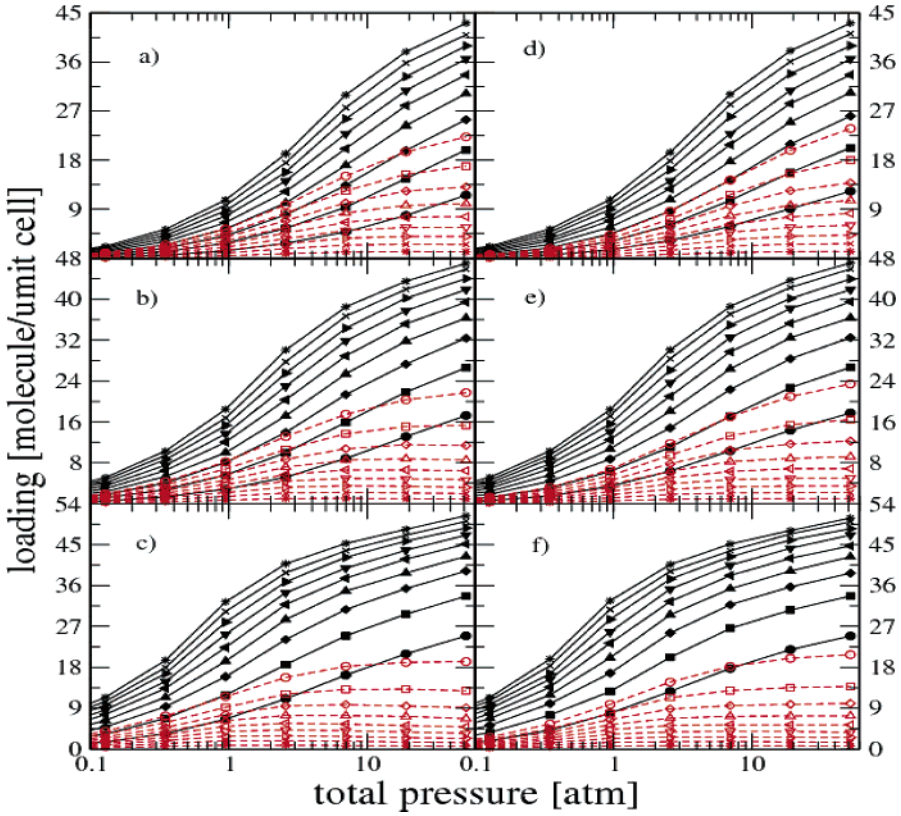

Figure 9. Full zeolite sorption isotherms of carbon dioxide/methane mixtures: (a) 300 K CO_2/DCVKMS; (b) 275 K CO_2/DCVKMS; (c) 250 K CO_2/DCVKMS; (d) 300 K CO_2/GWMWQ; (e) 275 K CO_2/GWMWQ;and (f) 250 K CO_2/GWMWQ. Filled symbols and solid lines: CO_2 isotherms; open symbols and dashed lines: CH_4 isotherms. Carbon dioxide mole fractions in the gas phase $y_{CO_2} = 0.1$ (circles), 0.2 (squares), 0.3 (diamonds), 0.4 (up triangles), 0.5 (left triangles), 0.6 (down triangles), 0.7 (right triangles), 0.8 (crosses), and 0.9 (stars).

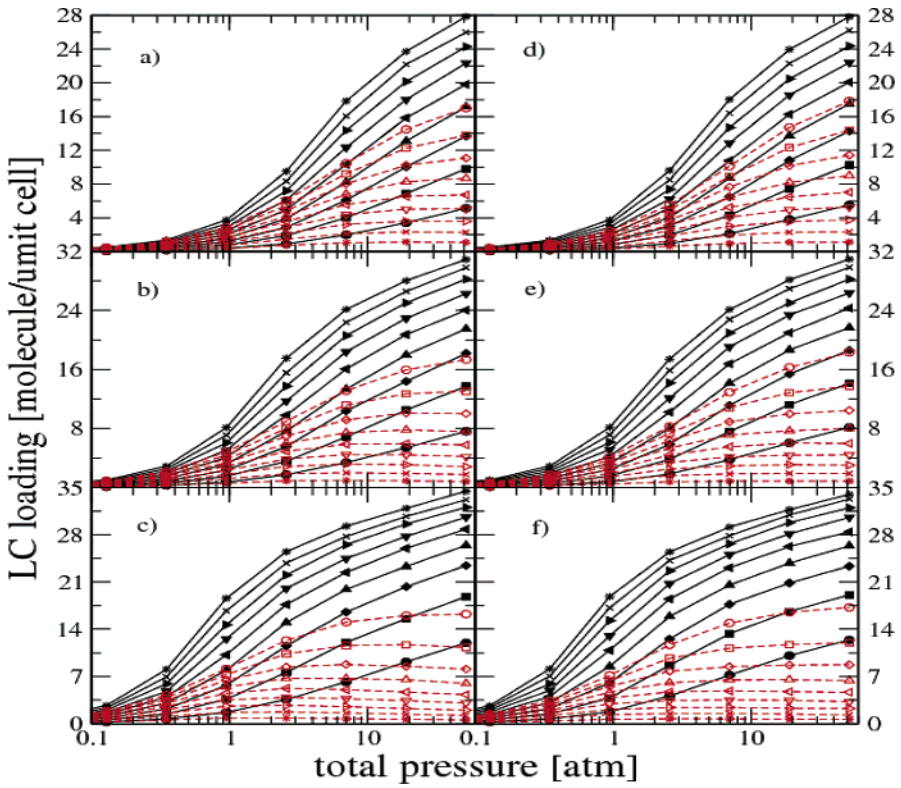

Figure 10. Identical with Figure 9 for the LC sorption.

methane. We can see in Figure 13 than the presence of CO_2 strongly affects (decreases) the sorption of CH_4 in both pore systems of the zeolite, sorption being more affected in SC than in LC. In particular, we see that, while the total loading in the limit of high pressures is between 30 and 40 (depending on temperature and model) molecules per unit cell for pure CH_4, it is reduced to between 18 and 24 for a mixture with a CO_2 mole fraction of only 0.1. At $T = 250$ K, the total loading at

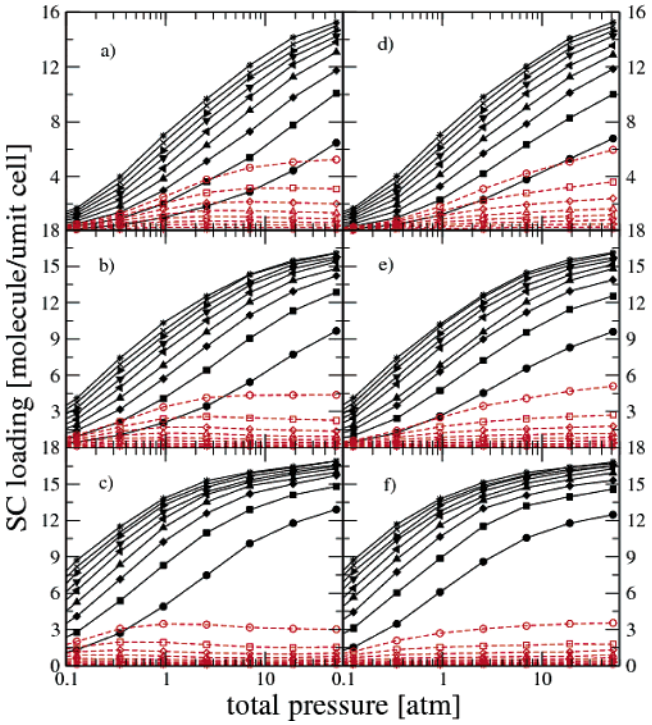

Figure 11. Identical with Figure 9 for the SC sorption.

high pressure for such a mixture is only half of the pure compound value. The SC loading at high pressure and $T = 250$ K for a CO_2 mole fraction of 0.1 is only one-third or one-fourth (depending on the model) of the pure methane loading.

We now discuss in a more quantitative way the selectivity of the zeolite with respect to carbon dioxide/methane gas mixtures by computing the selectivity factor S, defined by Nicholson and Gubbins,[32] as

$$S = \left(\frac{x_{CO_2}}{x_{CH_4}}\right)\left(\frac{y_{CH_4}}{y_{CO_2}}\right)$$

In this equation x_i and y_i are the mole fractions of compound i in the zeolite and the gas phase, respectively. Note that in the Henry regime S is identical with the ratio of the Henry constants of the two compounds. The selectivity isotherms corresponding to the sorption isotherms of Figures 9, 10, and 11 are shown in Figures 14, 15, and 16, respectively. The first point to note is that the zeolite is CO_2-selective for all temperatures, pressures, and compositions, since the selectivity factor S is always greater than unity. We can also see from Figure 14 that, despite the fact that the low-pressure selectivities differ quite a lot for the two methane models (due to different Henry constants), the values obtained at saturation are very similar and clearly higher than the one obtained at low pressure. Another common trend observed with the two models is that the richer in CO_2 the gas phase is, the stronger the increase of selectivity with pressure at low pressure. The evolution of selectivity with pressure is, however, not monotonic and we can see that most of the curves exhibit a selectivity maximum followed by a minimum. This effect is particularly noticeable in the case of a CO_2-rich gas phase. At saturation, the richer in CO_2 the gas phase is, the lower the selectivity. Note that this difference in selectivity at saturation is far from negligible. The origin of the nonmonotonic behavior of the selectivity isotherms is not easy to understand, since there is no direct mathematical relationship between the global selectivity and the LC and SC selectivities. We can see in Figure 15 that selectivity increases monotonically with

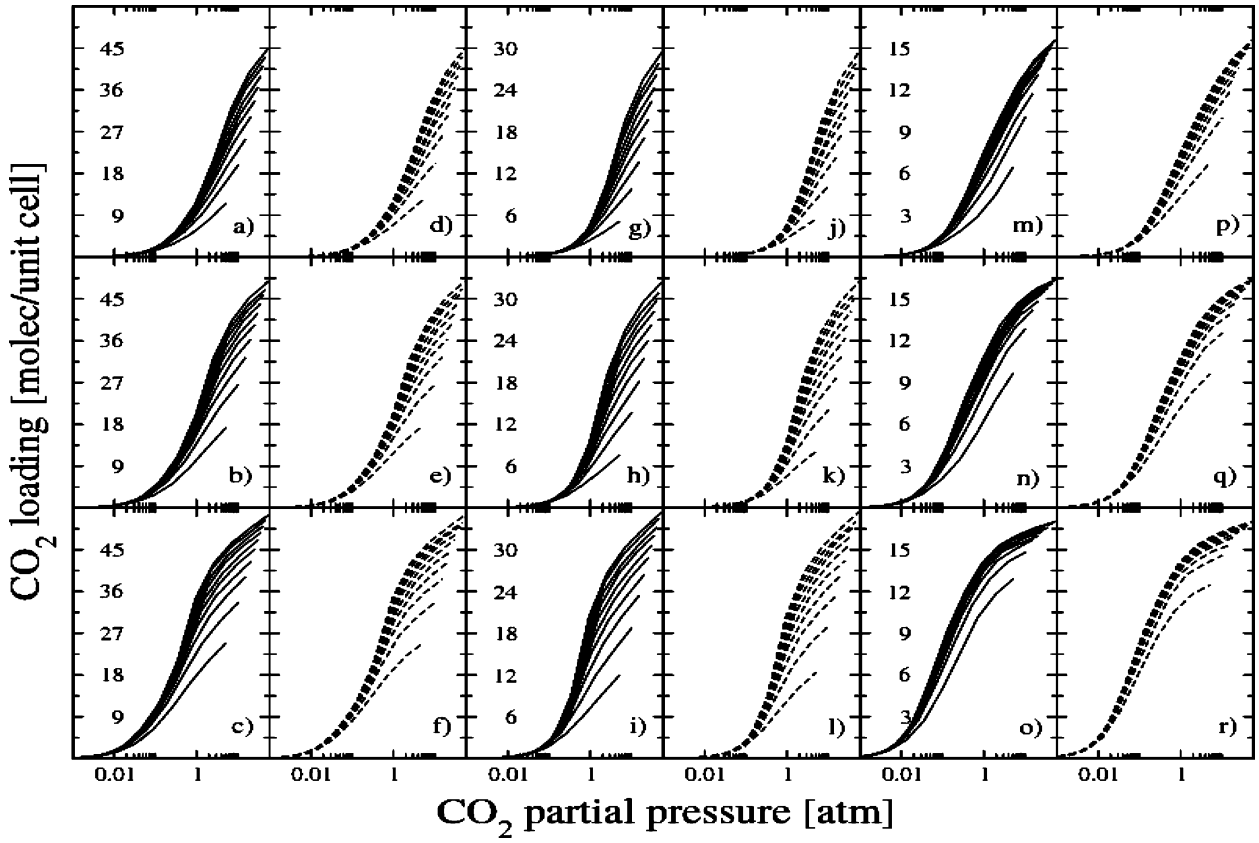

Figure 12. Evolution of the carbon dioxide loading with its partial pressure and with the gas-phase composition for CO_2/DCVKMS gas mixtures at 300 (a), 275 (b), and 300 K (c) and for CO_2/GWMWQ mixtures at 300 (d), 275 (e), and 250 K (f). (g−l): similar to (a−f) for the LC loading; (m−r): similar to (a−f) for the SC loading. On one graph, the carbon dioxide molar fractions evolve from 0.1 (bottom curve) to 1 (top curve).

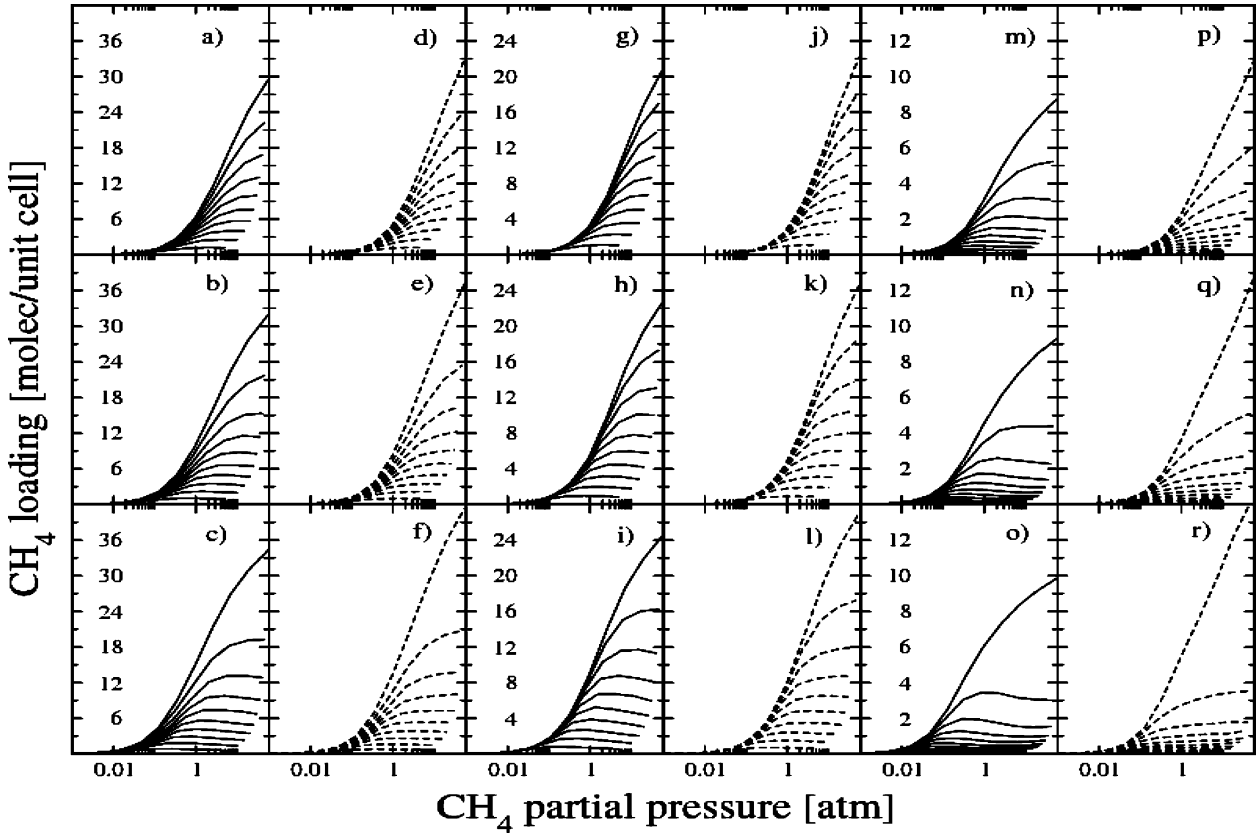

Figure 13. Similar to Figure 12 for the methane loading.

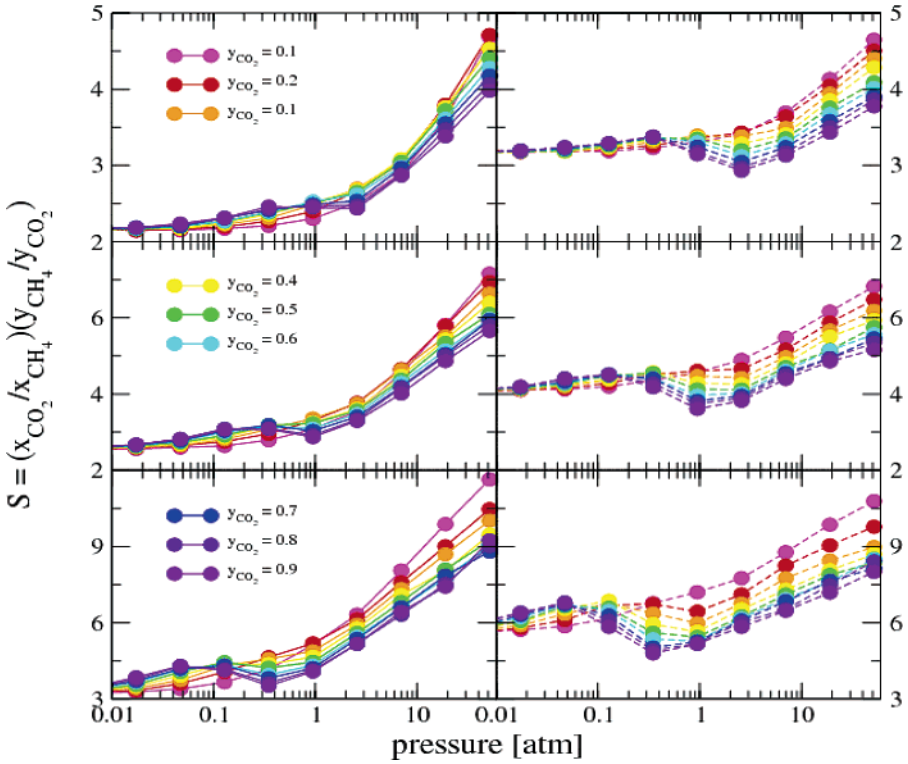

Figure 14. Full zeolite selectivity isotherms for CO_2/DCVKMS CH_4 (left) and CO_2/GWMWQ CH_4 (right) gas mixtures. Top curves: $T = 300$ K; middle curves: $T = 275$ K; bottom curves: $T = 250$ K.

pressure in LC and is not strongly affected by the gas composition. On the contrary, Figure 16 shows a clear dependence of selectivity on the gas composition in SC. We can also see in this figure that, similar to what has been observed for the global selectivity, selectivity in SC increases with y_{CO_2} at low pressure and decreases at high pressure. This inversion is due to the fact that selectivity isotherms exhibit a maximum and that the higher y_{CO_2} is, the lower the maximum selectivity pressure is. We note that selectivity is usually thought to be independent of the gas-phase composition and most

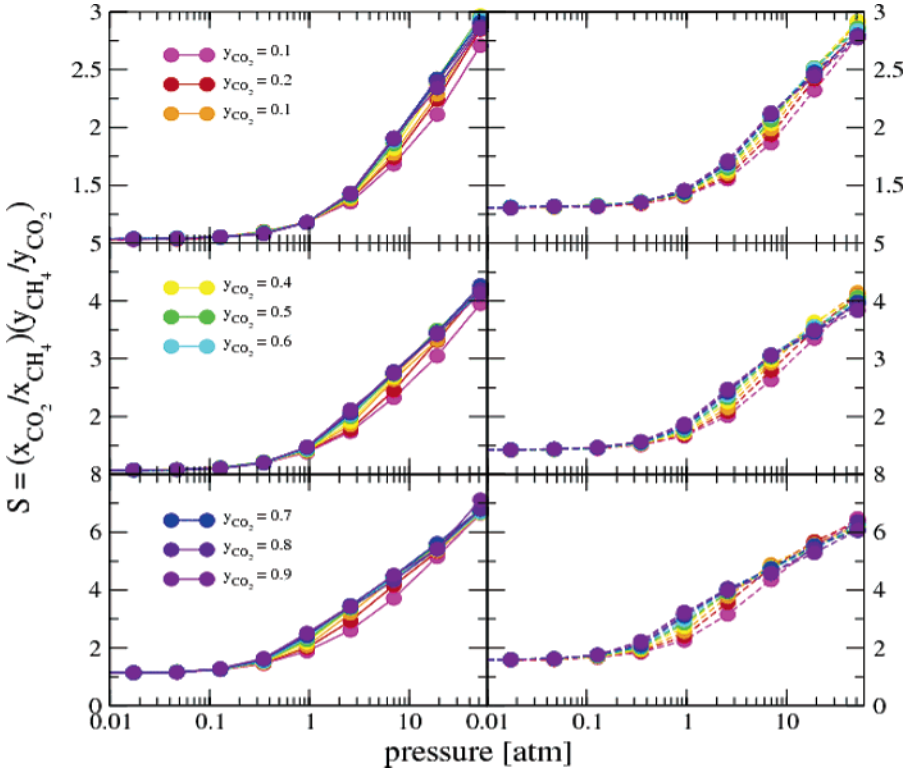

Figure 15. Similar to Figure 14 for the LC selectivity isotherms.

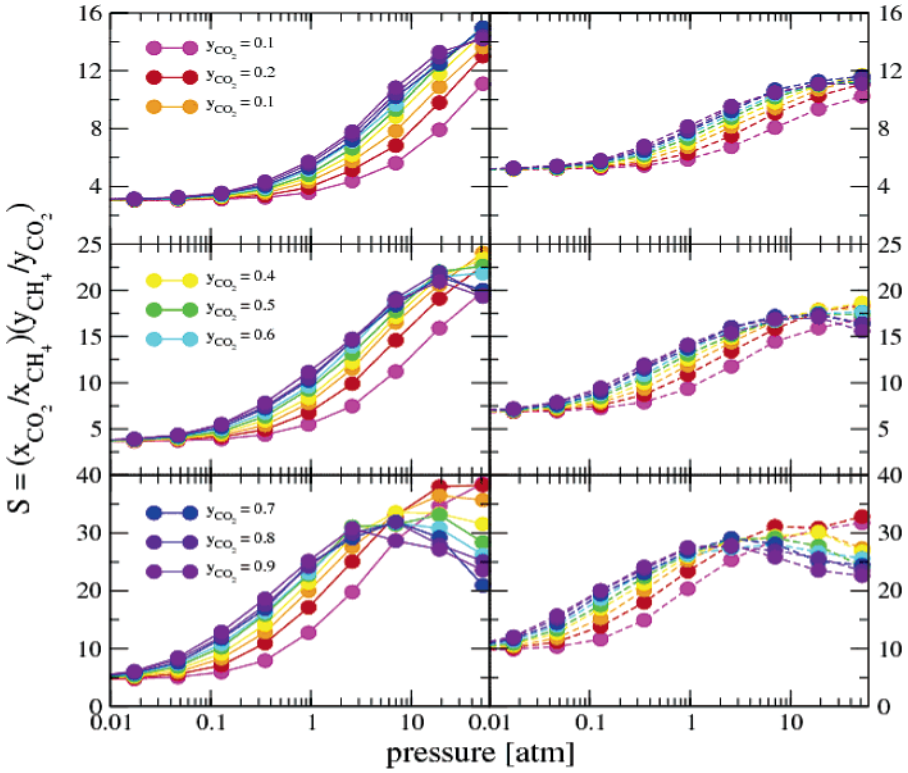

Figure 16. Similar to Figure 14 for the SC selectivity isotherms.

selectivity investigations are dealing with equimolar gas-phase composition.[33,34] In the case of a zeolite presenting two different and independent pore systems such as ITQ-1, however, high-pressure selectivity shows a dependence on the gas composition.

We now discuss in more detail the way in which the two components of the mixture distribute in space inside the zeolite. Figure 17 shows a snapshot of a configuration obtained during a GCMC simulation of a CO_2/DCVKMS CH_4 mixture with $y_{CO_2} = 0.1$ at $T = 250$ K and $P = 1$ atm. We choose this state point because it corresponds to a state at which the zeolite is filled but not saturated and because the total loadings of CO_2 and CH_4 have similar values. At this state point, CO_2 and CH_4 loadings are respectively 16.3 (6.2 in LC and 10.1 in SC) and 18.2 (15.0 in LC and 3.2 in SC) molecules per unit cell. An isodensity surface plot showing the areas of high sorbate density is superposed on the bottom right-hand side of the figure. We

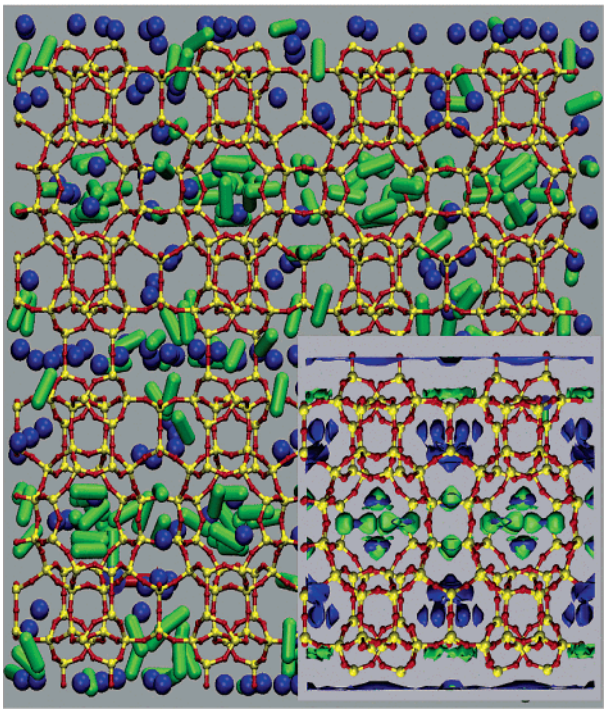

Figure 17. Snapshot of a configuration obtained in a GCMC simulation of a CO_2/DCVKMS CH_4 mixture at $T = 250$ K, $P = 7$ atm, and a gas-phase carbon dioxide mole fraction of 0.1. CO_2 molecules are displayed as light green sticks and methane as dark blue spheres. The inset (bottom right) shows high-density probability sites for carbon dioxide in green and methane in blue.

see clearly, in both the snapshot and the isodensity plot, that the two sorbates tend to occupy different sorption sites. Whereas methane is mainly sorbed in LC, in the top of the supercage pockets (LC1), close to the oxygen atoms of the 12 MR at the base of the LC (LC2) and in the intercavity space (LC3), carbon dioxide is mainly sorbed in SC and in the intermediate area between the top and base of LC. This is confirmed in Figure 18, which shows probability density plots for the two sorbates at this state point. The plot relative to carbon dioxide in LC (top left) shows strong peaks in the pocket areas and only very small peaks in the intercavity space (LC3). We see in the bottom left plot that methane occupies both pocket sites (LC1 and LC2) and intercavity sites (LC3). In SC, the CO_2 density plot (top right) shows the same feature observed for pure CO_2 at saturation (Figure 8b,c), characterizing strongly ordered sorbates in SC1 sites. Methane density in SC (inset at bottom right) is mainly located in SC1 sites, as for pure methane at low pressure.

5. Conclusions

Single-component and mixture adsorption properties of the carbon dioxide−methane in ITQ-1 zeolite system have been studied by Grand Canonical Monte Carlo simulations. We showed that both pore systems of the zeolite are CO_2 selective for all pressures, temperatures, and compositions investigated. Selectivity is also shown to increase considerably with pressure outside the Henry regime because of competitive adsorption. The sinusoidal channel pore system has been shown to be always more selective than the large cavity system. We found that selectivity is also slightly affected by the gas-phase composition, particularly in the sinusoidal channels. We showed that sorbate siting in the sorbent is considerably affected by the gas-phase pressure and composition. The maximum selectivity has been found to be at low-temperature, high-pressure, and methane-rich gas-phase composition. Under these conditions, we showed that CO_2 and CH_4 are not randomly located among the various sorbent sorption sites but reside in different preferential sites. Finally, we checked the reliability of our findings by comparing the sorption properties obtained with two different methane potential models from the literature. If the two potentials have led to some quantitatively different results, mainly at low pressure, they showed very similar qualitative trends. This paper was a first attempt to characterize the equilibrium selectivity of MWW materials with respect to CO_2/CH_4 gas mixtures. Transport properties of these mixtures in this zeolite are now under investigation to capture the kinetic aspects of a possible separation process. This work can now be extended to aluminated or chemically modified MCM-22 with an improvement of selectivity as a target.

Acknowledgment. Support by the European Union via the FP6-Marie Curie Research Training Network "INDENS" (MRTN-CT-2004-005503) is gratefully acknowledged.

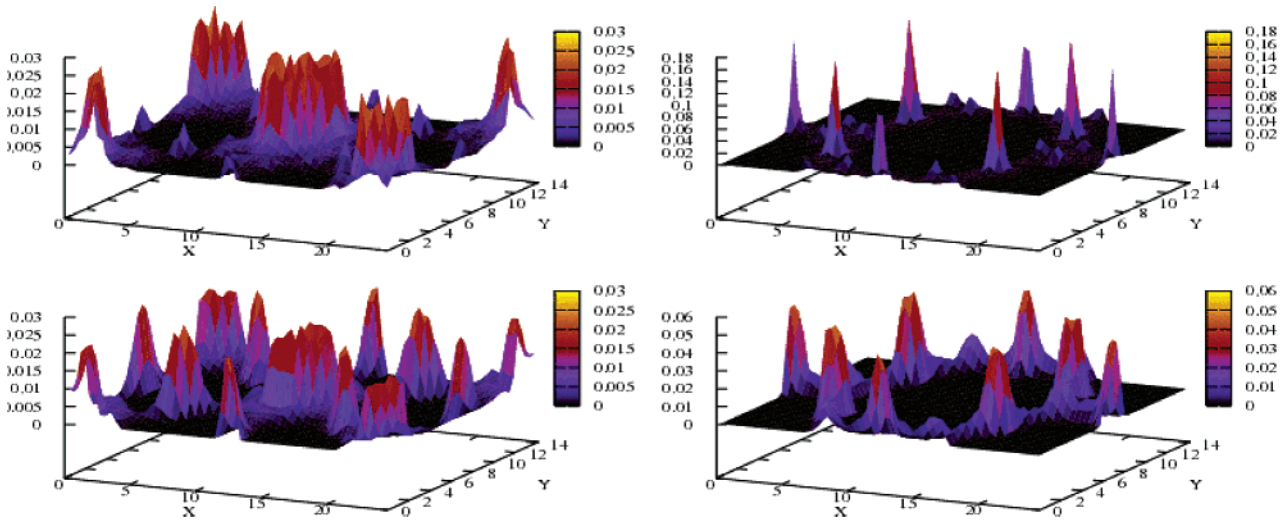

Figure 18. *xy* probability density plots at $T = 250$ K, $P = 7$ atm, and a gas-phase carbon dioxide mole fraction of 0.1. CO_2 in LC: top left; CH_4 in LC: bottom left; CO_2 in SC: top right; CH_4 in SC: bottom right.

References and Notes

(1) Koros, W. J.; Mahajan R. *J. Membr. Sci.* **2001**, *175*, 181.
(2) Ertl, G.; Knözinger, H.; Weitkamp, J., Eds. *Handbook of Heterogeneous Catalysis*; VCH: Weinheim, Germany, 1997.
(3) Yang, R. T. *Gas Separation by Adsorption Processes*; Butterworth: Boston, MA, 1987.
(4) Li, S.; Alvarado, G.; Noble, R. D.; Falconer, J. L. *J. Membr. Sci.* **2005**, *251*, 59.
(5) Li, S.; Martinek, J. G.; Falconer, J. L.; Noble, R. D.; Gardner, T. Q. *Ind. Eng. Chem. Res.* **2005**, *44*, 3220.
(6) Li, S.; Falconer, J. L.; Noble, R. D. *J. Membr. Sci.* **2004**, *241*, 121.
(7) Poshusta, J. C.; Noble, R. D.; Falconer, J. L. *J. Membr. Sci.* **2001**, *186*, 25.
(8) Poshusta, J. C.; Tuan, V. A.; Pape, E. A.; Noble, R. D.; Falconer, J. L. *AIChE J.* **2000**, *46*, 779.
(9) Tomita, T.; Nakayama, K.; Sakai, H. *Microporous Mesoporous Mater.* **2004**, *68*, 71.
(10) Hasegawa, Y.; Tanaka, T.; Watanabe, K.; Jeong, B. H.; Kusakabe, K.; Morooka, S. *Korean J. Chem. Eng.* **2002**, *19*, 309.
(11) Kusakabe, K.; Kuroda, T.; Murata, A.; Morooka, S. *Ind. Eng. Chem. Res.* **1997**, *36*, 649.
(12) Zhu, W.; Hrabanek, P.; Gora, L.; Kapeteijn, F.; Moulijn, J. A. *Ind. Eng. Chem. Res.* **2006**, *45*, 767.
(13) Gardner, T. Q.; Flores, A. I.; Noble, R. D.; Falconer, J. L. *AIChE J.* **2002**, *48*, 1155.
(14) Poshusta, J. C.; Noble, R. D.; Falconer, J. L. *J. Membr. Sci.* **1999**, *160*, 115.
(15) Takata, Y.; Tsuru, T.; Yoshioka, T.; Asaeda, M. *Microporous Mesoporous Mater.* **2002**, *54*, 257.
(16) van den Broeke, L. J. P.; Bakker, W. J. W.; Kapeteijn, F.; Moolijn, J. A. *Chem. Eng. Sci.* **1999**, *54*, 245.
(17) van den Broeke, L. J. P.; Kapeteijn, F.; Moolijn, J. A. *Chem. Eng. Sci.* **1999**, *54*, 259.
(18) Algieri, C.; Bernardo, P.; Golemme, G.; Barbieri, G.; Drioli, E. *J. Membr. Sci.* **2003**, *222*, 181.
(19) Bonhomme, F.; Welk, M. E.; Nenoff, T. M. *Microporous Mesoporous Mater.* **2003**, *66*, 181.
(20) Leonowicz, M. E.; Lawton, J. A.; Lawton, S. L.; Rubin, M. K. *Science* **1994**, *264*, 1910.
(21) Du, H.; Kalyanaraman, M.; Camblor, M. A.; Olson, D. H. *Microporous Mesoporous Mater.* **2000**, *40*, 305.
(22) Rubin, M. K.; Chu, P. U.S. Patent no. 4954325, 1990.
(23) Camblor, M. A.; Corma A.; Días-Cabañas M. J.; Baerlocher C. *J. Phys. Chem. B* **1998**, *102*, 44.
(24) Fuchs, A. H.; Cheetham, A. K. *J. Phys. Chem. B* **2001**, *105*, 7375.
(25) Makrodimitris, K.; Papadopoulos, G. K.; Theodorou, D. N. *J. Phys. Chem. B* **2001**, *105*, 777.
(26) Harris, J. G.; Yung, K. H. *J. Phys. Chem.* **1995**, *99*, 12021.
(27) Goodbody, S. J.; Watanabe, K.; MacGovan, D.; Walton, J. P. R. B.; Quirke, N. *J. Chem. Soc., Faraday Trans.* **1991**, *87*, 1951.
(28) Dubbeldam, D.; Calero, S.; Vlugt, T. J. H.; Krishna, R.; Maesen, T. L. M.; Smit, B. *J. Phys. Chem. B* **2004**, *108*, 12301.
(29) June, R. L.; Bell, A. T.; Theodorou, D. N. *J. Phys. Chem.* **1990**, *94*, 1508.
(30) Adams, D. J. *Mol. Phys.* **1974**, *28*, 1241.
(31) Adams, D. J. *Mol. Phys.* **1975**, *29*, 307.
(32) Llewellyn, P. Personal communication.
(33) Nicholson, D.; Gubbins, K. E. *J. Chem. Phys.* **1996**, *104*, 8126.
(34) Kluson, P.; Scaife, S. J. *Chem. Biochem. Eng. Q.* **2002**, *16*, 97.